Theoretical analysis of scalar relaxation in ^{13}C-DNP in liquids

Orlando, Tomas,[1,*] Kuprov, Ilya,[2] and Hiller, Markus[1]

[1]*ESR Spectroscopy Group, Max Planck Institute for Multidisciplinary Sciences, Göttingen, Germany*

[2]*School of Chemistry, University of Southampton, Southhampton, United Kingdom*

CONTENTS

HARD-SPHERE FORCE-FREE MODEL

When the electron-nuclear dipolar interaction is modulated by translational diffusion, the hard-sphere force-free model can be used to calculate the SDF associated with the dipole-dipole interaction. In this case, the two molecules are approximated as rigid spheres with the spin at center. The SDF is given by [1]:

$$J_{\mathrm{D}}(\omega,\tau_{\mathrm{D}}) = \frac{1+5z/8+z^2/8}{1+z+z^2/2+z^3/6+4z^4/81+z^5/81+z^6/648} \tag{1}$$

with z is $z=\sqrt{2\omega\tau_{\mathrm{D}}}$, where ω is the angular frequency of the spin at the given magnetic field, and τ_{D} is the correlation time for the translational diffusion. The latter can be also written as $\tau_{\mathrm{D}} = r_{\mathrm{d}}^2/(D_{\mathrm{s}}+D_{\mathrm{r,s}})$, where r_{d} is the distance of minimum approach, D_{s} is the

* tomas.orlando@mpinat.mpg.de

self-diffusion coefficient of the solvent and $D_{\mathrm{r,s}}$ is the diffusion coefficient of the radical in the solvent.

The contribution of the dipolar interaction to the nuclear relaxation is given by: $R_1^{\mathrm{D}} = k_D \cdot [7J_{\mathrm{D}}(\omega_{\mathrm{e}}, \tau_{\mathrm{D}}) + 3J_{\mathrm{D}}(\omega_{\mathrm{n}}, \tau_{\mathrm{D}})]$ where the prefactor is:

$$k_{\mathrm{D}} = \frac{32000\pi}{405} \left(\frac{\mu_0}{4\pi}\right)^2 \frac{N_A C \gamma_{\mathrm{n}}^2 g_{\mathrm{e}}^2 \mu_{\mathrm{B}}^2 S(S+1)}{r_{\mathrm{d}}(D_{\mathrm{s}} + D_{\mathrm{r,s}})} \,. \tag{2}$$

The hard-sphere force-free model was used to describe the dipolar interaction in the case of $CHCl_3$ doped with TEMPONE radical [2, 3]. Because the C-O distance strongly depends on the direction of approach of the $CHCl_3$ molecule to the radical (via Cl atom, or via H atom) [2], the SDF J_{D} can be written as a sum of two components:

$$J_{\mathrm{D}}^{\mathrm{CHCl_3}}(\omega_{\mathrm{e,n}}, \tau_{\mathrm{D}}) = \frac{3}{4} J_{\mathrm{D}}^{(\mathrm{Cl})}(\omega_{\mathrm{e,n}}, \tau_{\mathrm{D}}^{\mathrm{Cl}}) + \frac{1}{4} J_{\mathrm{D}}^{(\mathrm{H})}(\omega_{\mathrm{e,n}}, \tau_{\mathrm{D}}^{\mathrm{H}}) \tag{3}$$

where $\tau_{\mathrm{D}}^{\mathrm{Cl}}$= 53 ps and $\tau_{\mathrm{D}}^{\mathrm{H}}$= 39 ps.[3] The prefactors 3/4 and 1/4 are weighting factors that stem from the geometry of the $CHCl_3$ molecule, with three Cl atoms and one H atom bonded to the target C atom [2].

THE PULSE MODEL

The Pulse model, as described in the main text, can be written for an arbitrary shape of the pulses, each representing a collision between the two spins. In agreement with previous literature [2–4], we chose a Lorentzian pulse, which, comepared with the $A_{\mathrm{iso}}(t)$ traces obtained numerically, are a good approximation of the evolution $A_{\mathrm{iso}}(t)$ during a collision. Figure S1 shows a comparison of the scalar SDF $J_{\mathrm{SC,Pulse}}(\omega_{\mathrm{e}}, \tau_{\mathrm{SC}})$ calculated for different pulse shapes but with the same correlation time τ_{SC}. The full analytical treatment can be found in Ref. 5. Also, we considered a Lorentzian SDF, i.e. $J_{\mathrm{SC}}(\omega_{\mathrm{e}}, \tau_{\mathrm{SC}}) = \tau_{\mathrm{SC}}/(1 + \omega_{\mathrm{e}}^2 \tau_{\mathrm{SC}}^2)$.

BLOCH-REDFIELD-WANGSNESS (BRW) THEORY

All relaxation superoperators were computed using the numerical implementation [6, 7] of Bloch-Redfield-Wangsness (BRW) theory [8, 9] available in *Spinach* [10]. Separate treatments were performed for the rotational and the scalar collisional mechanisms, with the corresponding stochastic processes (rotational and translational diffusion) assumed to be uncorrelated.

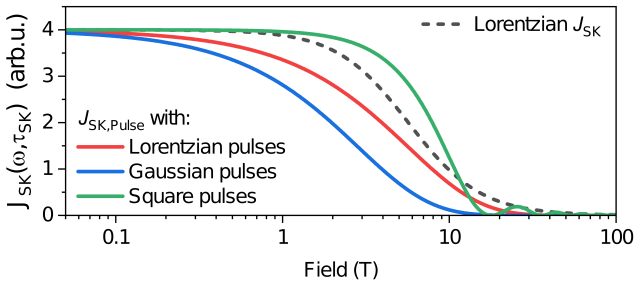

FIG. S1. SDFs $J_{\mathrm{SC,Pulse}}(\omega_{\mathrm{e}}, \tau_{\mathrm{SC}})$ as a function of the magnetic field calculated with the pulse model (solid lines) for different shapes of the collision pulse. The pulse duration is $\tau_{\mathrm{SC}} = 2$ ps and the prefactor has been arbitrarily chosen to rescale the SDFs to the same value at low fields. A Lorentzian SDF (dashed line) is shown for comparison.

For a system containing a nuclear and an electron spin, the laboratory frame Hamiltonian is:

$$\hat{H} = \hat{\vec{N}} \cdot \mathbf{Z}_{\mathrm{N}}(t) \cdot \vec{B} + \hat{\vec{E}} \cdot \mathbf{Z}_{\mathrm{E}}(t) \cdot \vec{B} + A_{\mathrm{iso}}(t) \hat{\vec{N}} \cdot \hat{\vec{E}} + \hat{\vec{N}} \cdot \mathbf{A}_{\mathrm{dip}}(t) \cdot \hat{\vec{E}} \tag{4}$$

where dots denote inner products, $\hat{\vec{N}} = \left[\hat{N}_{\mathrm{X}}, \hat{N}_{\mathrm{Y}}, \hat{N}_{\mathrm{Z}}\right]$ is a vector of Cartesian nuclear spin operators, $\hat{\vec{E}} = \left[\hat{E}_{\mathrm{X}}, \hat{E}_{\mathrm{Y}}, \hat{E}_{\mathrm{Z}}\right]$ is a vector of Cartesian electron spin operators, $\hat{B}$ is the magnetic induction, $\mathbf{Z}_{\mathrm{N}}$ is a 3x3 nuclear Zeeman interaction tensor (assumed rotationally modulated), A_{iso} is the isotropic part of the hyperfine coupling (collisional modulation assumed as described below), and $\mathbf{A}_{\mathrm{dip}}$ is a symmetric 3x3 matrix corresponding to the dipolar part of the hyperfine coupling (assumed rotationally modulated).

For the rotational part of the relaxation theory, the Hamiltonian in Eq. 4 was cast, using the functionality implemented in *Spinach* kernel, into the following form:

$$\hat{H}(t) = \hat{H}_{\mathrm{iso}} + \sum_{m,k=-2}^{2} \mathfrak{D}^{(2)}_{km}(t) \hat{Q}_{km} \tag{5}$$

where the isotropic part contains ensemble averages of Zeeman and hyperfine interactions, $\mathfrak{D}^{(2)}_{km}(t)$ are second rank Wigner D functions of molecular orientation, and $\hat{Q}_{km}$ are irreducible spherical components of the anisotropic Hamiltonian [6]. The integrals in the relaxation superoperator:

$$\hat{\hat{R}} = -\sum_{kmpq} \int_0^{+\infty} G_{kmpq}(\tau) \hat{\hat{Q}}_{km} \exp(-i\hat{\hat{H}}_0\tau) \hat{\hat{Q}}^{\dagger}_{km} \exp(i\hat{\hat{H}}_0\tau) \mathrm{d}\tau \tag{6}$$

were then taken numerically using the auxiliary matrix formalism [7]. Isotropic rotational

diffusion was assumed: in that case, the expression for the rotational correlation function is:

$$G_{kmpq}(\tau) = \left\langle \mathfrak{D}^{(2)}_{km}(0)\mathfrak{D}^{(2)\,*}_{pq}(\tau)\right\rangle = \frac{1}{5}\delta_{kp}\delta_{mq}\exp\left(-\frac{\tau}{\tau_{\mathrm{C}}}\right) \tag{7}$$

where angular brackets denote an ensemble average, and τ_{C} is the rotational correlation time.

For the collisional part of the relaxation theory, isotropic averages of both Zeeman interactions were used in the static part $\hat{H}_0$ of the Hamiltonian. The perturbation part contained the centered (the average was subtracted and also placed into $\hat{H}_0$) stochastic part of the isotropic hyperfine coupling:

$$\hat{H}_0 = \omega_{\mathrm{E}}\hat{E}_{\mathrm{Z}} + \omega_{\mathrm{N}}\hat{N}_{\mathrm{Z}} + a_0\hat{V}\,,\quad \hat{H}_1(t) = a_1(t)\hat{V} \tag{8}$$

where

$$\hat{V} = \hat{E}_{\mathrm{X}}\hat{N}_{\mathrm{X}} + \hat{E}_{\mathrm{Y}}\hat{N}_{\mathrm{Y}} + \hat{E}_{\mathrm{Z}}\hat{N}_{\mathrm{Z}}\,,\quad \langle a_1(t)\rangle = 0\,. \tag{9}$$

In this case, the standard BRW relaxation theory treatment yields [11]:

$$\hat{\hat{R}} = -\int_0^{+\infty}\langle a_1(t)a_1(t-\tau)\rangle\,\hat{\hat{V}}e^{-i\hat{\hat{H}}_0\tau}\hat{\hat{V}}e^{+i\hat{\hat{H}}_0\tau}\mathrm{d}\tau\,. \tag{10}$$

The autocorrelation function can be expressed as a linear combination of exponential decays with weights w_k and correlation times τ_k:

$$\langle a_1(t)a_1(t-\tau)\rangle = \Delta_{\mathrm{a}}^2\sum_k w_k\exp\left(-\frac{\tau}{\tau_k}\right) \tag{11}$$

where Δ_{a} is the amplitude of the time modulation of A_{iso} (in rad/s). When this expression is inserted into Eq. 10, it acquires the form that is amenable to the auxiliary matrix method for the numerical calculation of the matrix exponential integrals [7]. The functionality enabling the calculations described in this section is available in versions 2.7 and later of *Spinach* library [10]; the calculations presented in this work are included with the example set.

COUPLING FACTOR FROM BRW FORMALISM

Consider a two-spin system (S for the electron, I for the nucleus) and the corresponding four-level energy diagram (Figure 1 in the main text). The Solomon equations give the evolution of the I magnetization $\langle I_z\rangle$ as:

$$\frac{d\langle I_z\rangle}{dt} = -(w_0 + 2w_{1,\mathrm{I}} + w_2)(\langle I_z\rangle) - (w_2 - w_0)(\langle S_z\rangle - \langle S_z^{\mathrm{eq}}\rangle) \tag{12}$$

Solving for the steady-state $d\langle I_z\rangle/dt$=0, and adding the diamagnetic nuclear relaxation $w^0_{1,\mathrm{I}}$ leads to the Overhauser equation:

$$\langle I_z\rangle - \langle I_z^{\mathrm{eq}}\rangle = -\frac{w_2 - w_2}{w_0 + 2w_{1,\mathrm{I}} + w_2} \cdot \frac{w_0 + 2w_{1,\mathrm{I}} + w_2}{w_0 + 2w_{1,\mathrm{I}} + w^0_{1,\mathrm{I}} + w_2}(\langle S_z\rangle - \langle S_z^{\mathrm{eq}}\rangle) \tag{13}$$

where the two fractions are the coupling factor ξ and the leakage factor f, respectively.

The same situation can be described using the Liouville-von Neumann equation and the BRW formalism. In the Liouville space, the evolution of $\langle\hat{E}_z\rangle$ and $\langle\hat{I}_z\rangle$ is given by:

$$\frac{d}{dt}\begin{pmatrix}\langle\hat{E}_z\rangle\\ \langle\hat{N}_z\rangle\end{pmatrix} = \begin{pmatrix}-R_{1,\mathrm{E}} & \sigma\\ \sigma & -R_{1,\mathrm{N}}\end{pmatrix}\begin{pmatrix}\langle\hat{E}_z\rangle - \langle E_z^{\mathrm{eq}}\rangle\\ \langle\hat{N}_z\rangle - \langle N_z^{\mathrm{eq}}\rangle\end{pmatrix} \tag{14}$$

where $R_{1,(i)}$ is the electron (nuclear) longitudinal relaxation rate, σ is the cross relaxation rate, and $\langle E_z^{\mathrm{eq}}\rangle$, $\langle N_z^{\mathrm{eq}}\rangle$ are the electron and nuclear equilibrium states. Solving the equation for the steady state, one gets:

$$(\langle\hat{N}_z\rangle - \langle N_z^{\mathrm{eq}}\rangle) = \frac{\sigma}{R_{1,\mathrm{N}}}(\langle\hat{E}_z\rangle - \langle E_z^{\mathrm{eq}}\rangle)\,, \tag{15}$$

which is the analogue in the Liouville space of the Overhauser equation Eq. 13. Comparing Eq. 13 and Eq. 15 yields the following equivalence:

$$\xi f = \frac{\sigma}{R_{1,\mathrm{N}}} \xrightarrow{f\sim 1} \xi \sim \frac{\sigma}{R_{1,\mathrm{N}}}\,. \tag{16}$$

MOLECULAR DYNAMICS AND DFT

The dynamics of the interaction of the TEMPONE radical with $CHCl_3$ were probed by MD simulations using Gromacs 2018.4 [12]. For the radical, the force field parameters (compatible with the Amber99* force field) were adopted from the literature [13]. Bond and angle parameters for chloroform were chosen in agreement with the Amber force field parameters, atomic charges were obtained by geometry optimization (Orca 4.0.1, HF/6-31g*) and subsequent fitting using the RESP methodology [14] as implemented in Multiwfn 3.6 [15]. This approach, which has been reported before in detail for chloroform [16] was found to yield excellent agreement with previous literature reports [17].

The MD system was prepared by constructing a box containing a TEMPONE radical and a number of solvent molecules (1348 for $CHCl_3$). The systems were equilibrated for 500 ps in the NVT and NPT ensembles, respectively. Following this, the MD trajectories

used for analysis were recorded by saving the molecular coordinates in 0.2 ps intervals. The total length of the trajectory was 10 ns for $CHCl_3$. For the analysis of the time-dependence of the hyperfine interaction, subsets of both trajectories were used. For chloroform, two datasets were created, one covering the first 100 ps (dataset S, "short") and one covering the range from 1000-2000 ps (dataset L, "long"). In order to obtain the hyperfine couplings, DFT calculations were performed for the individual structures in the datasets, retaining only the three solvent molecules closest to the radical. Since a large number of calculations is required for this (5001 calculations for the dataset L), the creation of DFT input files and analysis of DFT output files was automated by a Python script. For the computations, Orca 4.2.1 was used employing the BLYP functional in conjunction with the EPR-II basis sets for C and H atoms and the IGLO-II basis set for Cl atoms [18]. Single point calculations were carried out using Tight SCF convergence criteria and the isotropic hyperfine interactions were calculated for the C and H atoms in $CHCl_3$. The traces of the hyperfine interactions were constructed by taking the DFT-derived values for the C atoms in the molecules contained in the DFT system (i.e. the closest three) and assuming a value of 0 for the remaining ones.

$A_{\mathbf{iso}}(t)$ TRACES AND AUTOCORRELATION FUNCTIONS

The $A_{\mathrm{iso}}(t)$ traces were used to numerically calculate the SDF for the scalar interaction. The autocorrelation function for each trace $A_{\mathrm{iso},m}(t)$ is

$$K_m(t) = \frac{4\pi^2}{N}\langle A_{\mathrm{iso},m}(\tau) \cdot A_{\mathrm{iso},m}(\tau + t)\rangle_\tau \tag{17}$$

where $4\pi^2$ converts $K(t)$ into angular frequency units and N is the number of target nuclei per radical over the the volume. In the $CHCl_3$ case, we had 1348 $CHCl_3$ molecules in a 204.7 nm^3 box. Numerically, the autocorrelation function can be computed with Matlab (function `xcorr.m`). The $K_m(t)$ calculated for $A_{\mathrm{iso},m}(t)$ traces for $CHCl_3$ and TEMPONE are shown in Figure S3, where only the positive part of the time axis ($t > 0$) is considered ($K_m(t)$ is symmetric).

The sum of the autocorrelation functions $K(t) = \sum_m K_m(t)$ is shown Figure S3. The SDF can be calculated from the autocorrelation $K(t)$ as the one-sided Fourier transform, i.e.:

$$J_{\mathrm{SC}}(\omega) = \int_0^{+\infty} K(t)\exp(-i\omega t)dt \tag{18}$$

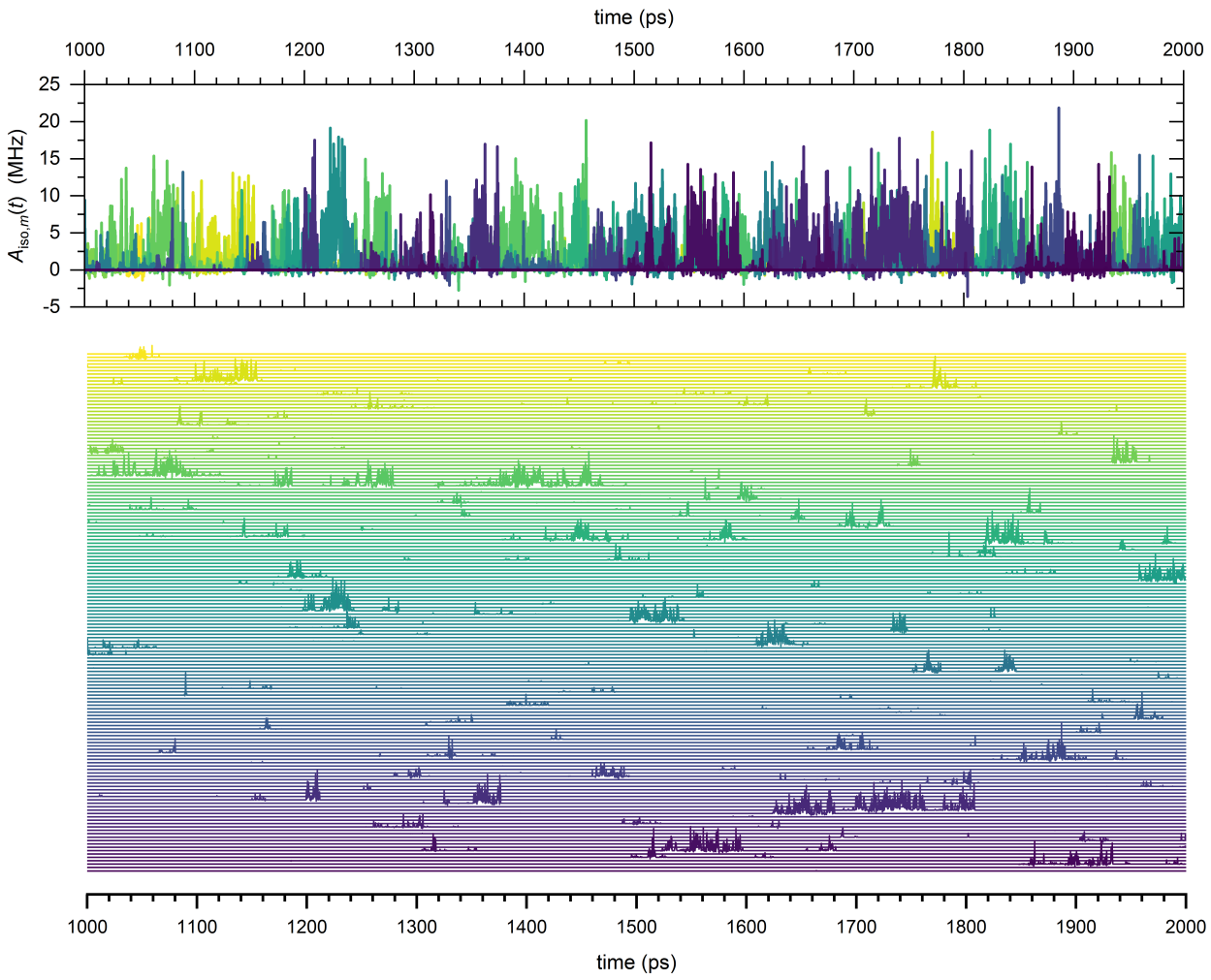

FIG. S2. $A_{\mathrm{iso},m}(t)$ traces recorded in the time interval 1000-2000 ps (dataset L). Of the 1348 traces, 154 have $A_{\mathrm{iso}} \neq 0$ for at least one time point in the selected time interval. Those are the one shown here (top panel: overlapped traces; bottom panel: stacked traces).

NUMERICAL FOURIER TRANSFORM OF $K(t)$

Figure S3 shows $J_{\mathrm{SC}}(\omega)$ calculated numerically from $K(t)$. The frequency range $[\nu_{\mathrm{min}}, \nu_{\mathrm{max}}]$ is a function of the sampling time t_{samp} of the autocorrelation function $K(t)$, which is, by definition, equal to the time step used to record the trace $A_{\mathrm{iso}}(t)$. Therefore, one has:

$$\nu_{\mathrm{min}} = \frac{1}{t_{\mathrm{samp}}} \frac{1}{n} \; ; \; \nu_{\mathrm{max}} = \frac{1}{2t_{\mathrm{samp}}} \tag{19}$$

where n is the number of points of $K(t)$ (equal to the number of points of the trace $A_{\mathrm{iso}}(t)$. In the case of $CHCl_3$, $A_{\mathrm{iso}}(t)$ for dataset S was sampled in the range 0-100 ps with t_{samp}= 0.2 ps and n= 500 points: these lead to ν_{min}= 10 GHz and ν_{max}= 2500 GHz (Figure S3).

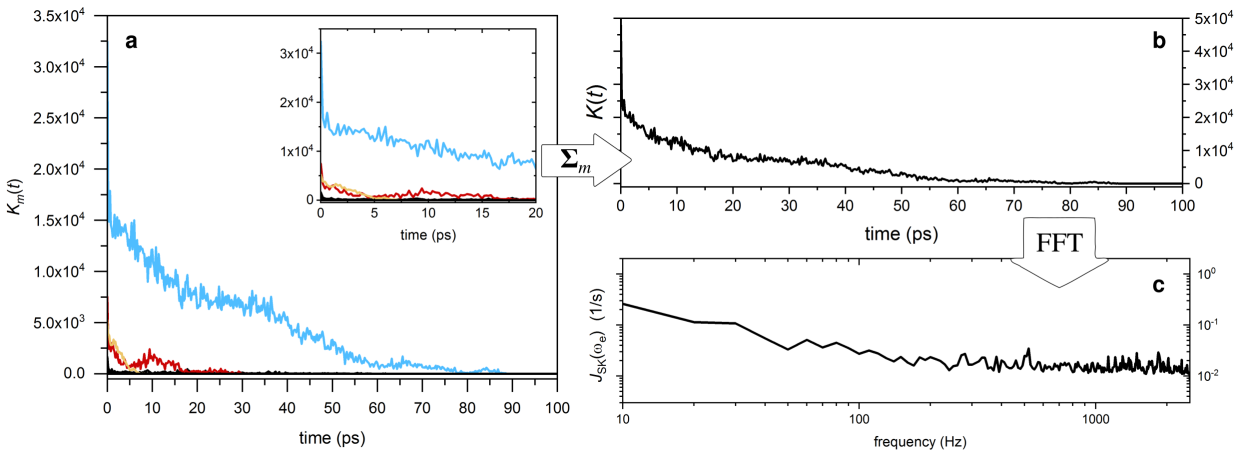

FIG. S3. **a)** Autocorrelation functions $K_m(t)$ calculated for the traces $A_{\mathrm{iso},m}(t)$ of dataset S. The color code is the same used for the traces in the main text. **b)** Sum of the autocorrelation functions $K_m(t)$ from dataset S. **c)** SDF calculated as one-sided Fourier transform of $K(t)$.

A longer trace of 1 ns was recorded for dataset L, in the interval 1000-2000 ps: in this case, the SDF covers the a larger frequency range 1–2500 GHz.

The SDF $J_{\mathrm{SC}}(\omega)$ was calculated as the Fourier transform of $K(t)$ using the FFT algorithm (the same results were obtained with Origin and Matlab).The same algorithm was used to calculate the Fourier transform of the function $K_{\mathrm{fit}}(t) = c_0 + \sum_{i=1}^{4} c_i e^{-t/t_i}$ used to fit the function $K(T)$ (Figure S4). The latter was the calculated in the range 0–25000 ps with a time step of 0.05 ps, much shorter than the time step used for sampling $K(t)$. The fit parameters are $[c_1 = 1.84 \cdot 10^5, t_1 = 19.1]$, $[c_2 = 9.97 \cdot 10^4, t_2 = 1.78]$, $[c_3 = 2.92 \cdot 10^4, t_3 = 124]$, $[c_4 = 2.05 \cdot 10^5, t_4 = 0.108]$, where the decay times are given in ps. The numerical Fourier transforms $\mathrm{FFT}(K(t))$ and $\mathrm{FFT}(K_{\mathrm{fit}}(t))$ are compared in Figure S4. A larger sampling rate leads to an overestimation of the SDF $J_{\mathrm{SC}}(\omega)$ in the high field region (B>10 T).

To check the reproducibility of the results, the analysis of the traces $A_{\mathrm{iso}}(t)$ was performed for five different datasets extracted from the MD run. In particular, we considered five time ranges: A) 1000-2000 ps; B) 2000-3000 ps; C) 3000-4000 ps; D) 4000-5000 ps; E) 5000-6000 ps. The autocorrelation functions $K(t)$ were fitted with a sum of four exponential decays. The components with larger weights w_i have time constants t_i in the range 0.1-25 ps (Figure S5a). Despite small differences in the decay times t_i, the SDFs extracted from each trace are in excellent agreement (Figure S5b).

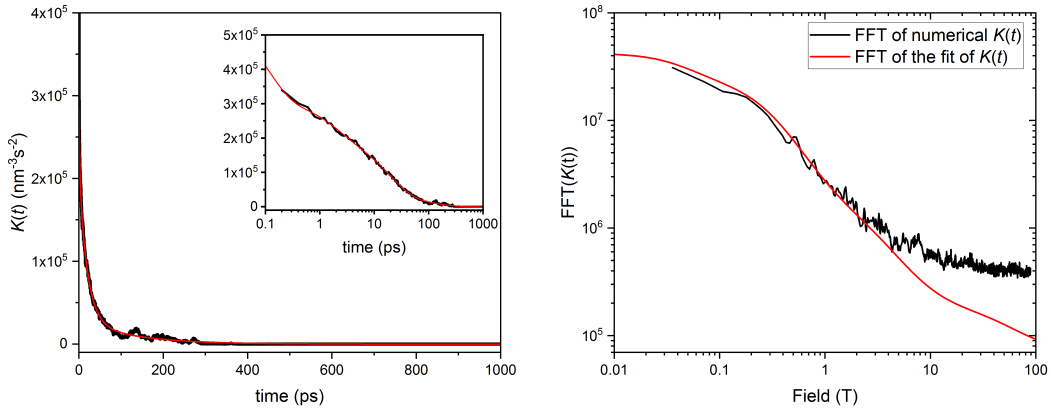

FIG. S4. a) Autocorrelation function $K(t)$ from the dataset L and fit performed with a sum of four exponential decays, i.e. $c_0 + \sum_{i=1}^{4} c_i e^{-t/t_i}$, where c_i and t_i are fitted parameters. The inset shows the same function in semi-logarithmic scale to highlight the region <1 ps. b) Numerical Fourier transforms via FFT of the function $K(t)$ and of its fit function $K_{\mathrm{iso}}(t)$.

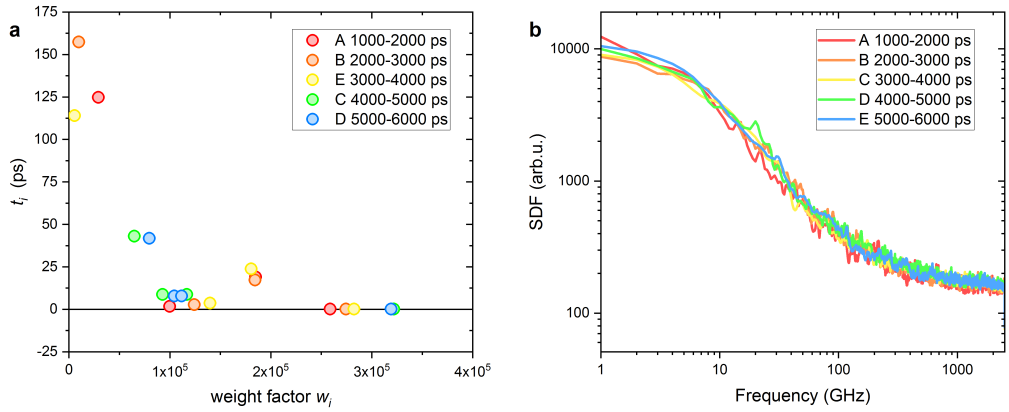

FIG. S5. a) Time constanst t_i as a function of their corresponding weight w_i extracted from the fit of four correlation functions $K(t)$ corresponding to different sections of the trace $A_{\mathrm{iso}}(t)$. b) SDFs obtained as numerical Fourier transforms of the autocorrelation functions $K(t)$.

NUCLEAR RELAXATION RATE $R_{1,\mathrm{SC}}$

Following the work of the Florence group [19–21], within the formalism of the relaxation theory, the coupling factor can be written as:

$$\xi = \frac{5k_{\mathrm{D}} \cdot J_{\mathrm{D}}(\omega_{\mathrm{e}}, \tau_{\mathrm{D}}) - R_{1,\mathrm{SC}}}{R_{1,\mathrm{para}}} \,. \tag{20}$$

where $R_{1,\mathrm{SC}} = k_{\mathrm{SC}} J_{\mathrm{SC}}(\omega_{\mathrm{e}}, \tau_{\mathrm{SC}})$ is the nuclear relaxation that originates from the electron-nuclear scalar interaction.

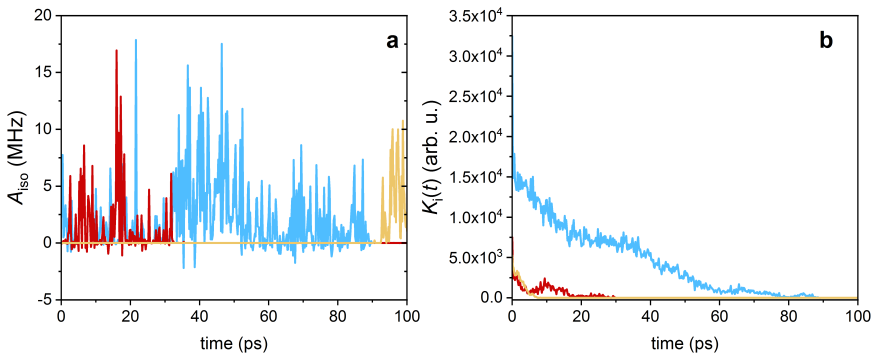

FIG. S6. Traces $A_{\mathrm{iso},m}(t)$ and corresponding autocorrelation functions $K_m(t)$ for the three $CHCl_3$ molecules that are forming a longer transient complex with the TEMPONE radical (dataset S). The color code is the same used in Figure S3 and in the traces shown in the main text.

The same equation can be rewritten in quantities that are computationally accessible, i.e. the spectral densities. This approach, described in Ref. 22 and 23, leads to:

$$\xi = \frac{5J_{\mathrm{D}}^{(\mathrm{Num.})}(\omega_{\mathrm{e}}) - 6J_{\mathrm{SC}}^{(\mathrm{Num.})}(\omega_{\mathrm{e}})}{3J_{\mathrm{D}}^{(\mathrm{Num.})}(\omega_{\mathrm{n}}) + 7J_{\mathrm{D}}^{(\mathrm{Num.})}(\omega_{\mathrm{e}}) + 6J_{\mathrm{SC}}^{(\mathrm{Num.})}(\omega_{\mathrm{e}})}\,, \tag{21}$$

where $J_{\mathrm{D}}^{(\mathrm{Num.})}(\omega_{\mathrm{e}})$ and $J_{\mathrm{SC}}^{(\mathrm{Num.})}(\omega_{\mathrm{e}})$ are the SDFs of the dipolar and scalar interactions, respectively, calculated numerically from MD/DFT simulations. From Eq. 20 and Eq. 21 it follows that $R_{1,\mathrm{SC}}^{(\mathrm{Num.})} = 6J_{\mathrm{SC}}^{(\mathrm{Num.})}(\omega_{\mathrm{e}})$.

RADICAL/$CHCl_3$ TRANSIENT COMPLEX

Some autocorrelation functions $K_m(t)$ from dataset S and dataset L (Figure S3) show high amplitudes. When selecting the autocorrelation functions that satisfy the condition $K_m(t^*) > 500$ with $t^* = 0.2\,\mathrm{ps}$, it becomes clear that the corresponding traces $A_{\mathrm{iso},m}(t)$ are those of the $CHCl_3$ molecules that are in a transient complex with the radical (Figure S6). The same can be done for the autocorrelation functions $K_m(t)$ from the dataset L: the traces $A_{\mathrm{iso},m}(t)$ corresponding to the largest $K_m(t)$ are shown in Figure S2.

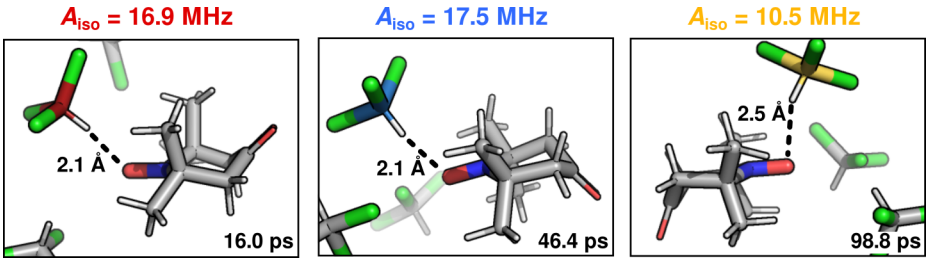

FIG. S7. Geometries of the complex $CHCl_3$/nitroxide for some of the largest values of A_{iso}. The closest C atom is color coded according to the traces in Figure S6 (atom color code: H white; C gray; N blue; O red; Cl green).

SPINACH SIMULATIONS

The numerical simulations were performed using *Spinach* [10]. The set of parameters that defines the two-spin system (electron-^{13}C) used for the simulations of the coupling factor is reported in Table I. To take into account the fast relaxation of the electron [24], we included an additional relaxation term for both spins with the following values: for the electron $T_{1,e}$= 500 ns, $T_{2,e}$= 200 ns [24]; for the ^{13}C nucleus $T_{1,n}$= 4.0 s, $T_{2,n}$= 0.3 s. The simulation with *Spinach* was performed with the relaxation modules redfield, t1_t2, and SRFK; for the latter, we used the labframe assumption set for both electrons and nuclei.

[1] L.-P. Hwang and J. H. Freed, Dynamic effects of pair correlation functions on spin relaxation by traslational diffusion in liquids, The Journal of Chemical Physics **63**, 4017 (1975).

[2] G. Liu, M. Levien, N. Karschin, G. Parigi, C. Luchinat, and M. Bennati, One-thousand-fold enhancement of high field liquid nuclear magnetic resonance signals at room temperature, Nature Chemistry **9**, 676 (2017).

[3] T. Orlando, R. Dervişoğlu, M. Levien, I. Tkach, T. F. Prisner, L. B. Andreas, V. P. Denysenkov, and M. Bennati, Dynamic Nuclear Polarization of ^{13}C Nuclei in the Liquid State over a 10 Tesla Field Range, Angewandte Chemie - International Edition **58**, 1402 (2019).

[4] W. Müller-Warmuth, R. Vilhjalmsson, P. Gerlof, J. Smidt, and J. Trommel, Intermolecular interactions of benzene and carbon tetrachloride with selected free radicals in solution as studied by ^{13}C and ^{1}H dynamic nuclear polarization, Molecular Physics **31**, 1055 (1976).

TABLE I. Set of parameters that defines the two-spin system (electron-^{13}C) for the numerical BRW simulations with *Spinach*.

Parameter	**Value**
Electron g-tensor	[2.0098 2.0065 2.0029] [μ_B]
^{13}C CSA	[100 120 120] [ppm]
A_{iso}	2.0 [MHz]
electron-nuclear distance	3.1 [Å]
τ_{C} (rotational)	30 [ps]
Temperature	298 [K]
Scalar relaxation	
Δ_{a}	3.6 [MHz]
$[w_1, \tau_1]$	[0.38, 0.8] [–, ps]
$[w_2, \tau_2]$	[0.62, 30] [–, ps]

[5] F. Noack, G. J. Krüger, W. Müller-Warmuth, and R. Van Steenwinkel, Stochastische Prozesse in Spinsystemen, Zeitschrift fur Naturforschung - Section A Journal of Physical Sciences **22**, 2102 (1967).

[6] I. Kuprov, Diagonalization-free implementation of spin relaxation theory for large spin systems, Journal of Magnetic Resonance **209**, 31 (2011).

[7] D. L. Goodwin and I. Kuprov, Auxiliary matrix formalism for interaction representation transformations, optimal control, and spin relaxation theories, The Journal of Chemical Physics **143**, 084113 (2015).

[8] R. K. Wangsness and F. Bloch, The dynamical theory of nuclear induction, Phys. Rev. **89**, 728 (1953).

[9] A. G. Redfield, On the theory of relaxation processes, IBM Journal of Research and Development **1**, 19 (1957).

[10] H. J. Hogben, M. Krzystyniak, G. T. Charnock, P. J. Hore, and I. Kuprov, Spinach - A software library for simulation of spin dynamics in large spin systems, Journal of Magnetic Resonance **208**, 179 (2011).

[11] I. Kuprov, D. M. Hodgson, J. Kloesges, C. I. Pearson, B. Odell, and T. D. W. Claridge, Anomalous Nuclear Overhauser Effects in Carbon-Substituted Aziridines: Scalar Cross-Relaxation of the First Kind, Angewandte Chemie **127**, 3768 (2015).

[12] S. Pronk, S. Páll, R. Schulz, P. Larsson, P. Bjelkmar, R. Apostolov, M. R. Shirts, J. C. Smith, P. M. Kasson, D. van der Spoel, B. Hess, and E. Lindahl, GROMACS 4.5: a high-throughput and highly parallel open source molecular simulation toolkit, Bioinformatics **29**, 845 (2013).

[13] E. Stendardo, A. Pedone, P. Cimino, M. Cristina Menziani, O. Crescenzi, and V. Barone, Extension of the amber force-field for the study of large nitroxides in condensed phases: an ab initio parameterization, Physical Chemistry Chemical Physics **12**, 11697 (2010).

[14] C. I. Bayly, P. Cieplak, W. Cornell, and P. A. Kollman, A well-behaved electrostatic potential based method using charge restraints for deriving atomic charges: the resp model, The Journal of Physical Chemistry **97**, 10269 (1993).

[15] T. Lu and F. Chen, Multiwfn: A multifunctional wavefunction analyzer, Journal of Computational Chemistry **33**, 580 (2012).

[16] M. Levien, M. Hiller, I. Tkach, M. Bennati, and T. Orlando, Nitroxide Derivatives for Dynamic Nuclear Polarization in Liquids: the Role of Rotational Diffusion, The Journal of Physical Chemistry Letters **11**, 1629 (2020).

[17] T. Fox and P. A. Kollman, Application of the resp methodology in the parametrization of organic solvents, The Journal of Physical Chemistry B **102**, 8070 (1998).

[18] S. E. Küçük and D. Sezer, Multiscale computational modeling of ^{13}C dnp in liquids, Physical Chemistry Chemical Physics **18**, 9353 (2016).

[19] M. Bennati, C. Luchinat, G. Parigi, and M. T. Türke, Water ^{1}H relaxation dispersion analysis on a nitroxide radical provides information on the maximal signal enhancement in Overhauser dynamic nuclear polarization experiments, Physical Chemistry Chemical Physics **12**, 5902 (2010).

[20] E. Ravera, C. Luchinat, and G. Parigi, Basic facts and perspectives of Overhauser DNP NMR, Journal of Magnetic Resonance **264**, 78 (2016).

[21] G. Parigi, E. Ravera, M. Bennati, and C. Luchinat, Understanding Overhauser Dynamic Nuclear Polarisation through NMR relaxometry, Molecular Physics **117**, 888 (2019).

[22] D. Sezer, M. J. Prandolini, and T. F. Prisner, Dynamic nuclear polarization coupling factors calculated from molecular dynamics simulations of a nitroxide radical in water, Physical

Chemistry Chemical Physics **11**, 6626 (2009).

[23] S. E. Kü çük, T. Biktagirov, and D. Sezer, Carbon and proton Overhauser DNP from MD simulations and ab initio calculations: TEMPOL in acetone, Physical Chemistry Chemical Physics **17**, 24874 (2015).

[24] J. R. Biller, H. Elajaili, V. Meyer, G. M. Rosen, S. S. Eaton, and G. R. Eaton, Electron spin-lattice relaxation mechanisms of rapidly-tumbling nitroxide radicals, Journal of Magnetic Resonance **236**, 47 (2013).